1-31-2019

CoB6 Monolayer: A Robust Two-dimensional Ferromagnet

Xiao Tang
Queensland University of Technology

Weiguo Sun
Sichuan University

Yuantong Gu
Queensland University of Technology

Cheng Lu
University of Nevada, Las Vegas, cheng.lu@unlv.edu

Liangzhi Kou
University of Nevada, Las Vegas, Liangzhi.kou@qut.edu.au

See next page for additional authors

CoB_6 monolayer: A robust two-dimensional ferromagnet

Xiao Tang,[1] Weiguo Sun,[2] Yuantong Gu,[1] Cheng Lu,[3,*] Liangzhi Kou,[1,†] and Changfeng Chen[3,‡]
[1]*School of Chemistry, Physics and Mechanical Engineering, Queensland University of Technology, Gardens Point Campus, Brisbane, Queensland 4001, Australia*
[2]*Institute of Atomic and Molecular Physics, Sichuan University, Chengdu 610065, China*
[3]*Department of Physics and Astronomy, University of Nevada, Las Vegas, Nevada 89154, USA*

(Received 7 September 2018; revised manuscript received 20 November 2018; published 31 January 2019)

Two-dimensional (2D) magnetic materials are essential to developing high-performance spintronic devices. Recent experimental discoveries of several atomic thin 2D ferromagnetic materials have stimulated great interest in further exploring this fascinating class of materials. Here, combining an advanced crystal structure search method and extensive first-principles energetic and dynamic calculations, we have identified a planar CoB_6 monolayer as a stable 2D ferromagnet. We show that the ferromagnetic ground state of the CoB_6 monolayer remains robust in the ambient environment, and the magnetic stability and moment can be remarkably enhanced and tuned by external strain. Moreover, we propose feasible synthesis routes for the the newly predicted CoB_6 monolayer, either by Co atom adsorption on the recently proposed δ_4 boron sheet or by direct chemical growth. The present results establish a fundamental material and physics basis for synthesis and characterization of the CoB_6 monolayer among the emerging 2D ferromagnetic materials.

DOI: 10.1103/PhysRevB.99.045445

I. INTRODUCTION

Spintronics utilizes electron spin instead of charge for information storage, transport, and processing, and it holds great promise for next-generation high-performance devices with superior characteristics such as high processing speed and low power consumption. Research and development in the materials physics fields related to spintronics have attracted intensive interest from both fundamental and practical sides in recent decades [1]. Practical materials for spintronic applications should possess strong structural and magnetic stability, high Curie temperature, high spin polarization ratio, and feasibility for experimental fabrication. Recent studies have predicted a number of nanoscale ferromagnetic materials, such as the Fe_2Si sheet [2], MXene [3], strained NbS_2 and $NbSe_2$ [4], and defective or partially hydrogenated graphene [5–7]; however, ferromagnetic materials that meet the criteria for practical device implementation have been difficult to obtain due to challenges in material synthesis and stability. For example, although graphene is the most prominently predicted 2D magnetic material when vacancies or zigzag edges are present, it is rarely observed in experiment due to electron delocalization and other issues. Recent experimental progress has led to a breakthrough in the synthesis of truly 2D magnets, realized in pristine $Cr_2Ge_2Te_6$ [8], CrI_3 [9,10], and VSe_2 [11] atomic thin layers. The control of the transition temperatures between ferromagnetic and paramagnetic states has been achieved under small fields. More interestingly, the magnetism of a 2D CrI_3 layer has been shown to be controllable by electrostatic doping and external electric fields [12,13]. These experimental advances demonstrate the feasibility of the long-sought truly 2D magnets, thereby opening an exciting area of research for exploring additional 2D magnetic materials that exhibit similar or improved material characteristics, such as enhanced structural stability and magnetic transition temperature, that are crucial to device applications.

Boron nanostructures are a promising candidate materials for spintronic applications since they are highly susceptible to metal doping due to the electron deficiency of boron atoms. Boron rings containing central transition-metal atoms that form planar hexa-, hepta-, octa-, and higher coordination with the surrounding boron atoms, such as FeB_8, FeB_9, CoB_8, RuB_9, RhB_9, IrB_9, and VB_9 clusters [14–17], have been revealed by theoretical and experimental investigations. The transition-metal atoms not only can stabilize boron clusters via electron compensation, but also may induce magnetic order in the system. Based on experimentally revealed hypercoordinated planar born clusters, corresponding 2D layered materials have been theoretically proposed, and their magnetic ground states have been predicted in the planar hypercoordinated 2D iron boride FeB_x ($x = 2$–10) alloys [18] and MnB_x ($x = 1, 2, 3, 6$) layers [19,20]. However, although cobalt has been shown to form hypercoordination with boron frameworks, as demonstrated by recently synthesized planar CoB_8^-, CoB_{12}^-, CoB_{16}^-, and CoB_{18}^- clusters [21,22], hypercoordinated Co-B 2D layers have not been realized. Questions remain on whether such 2D layers can exist or if the Co atoms can induce magnetic orders. Another motivation for the study of embedding transition-metal atoms into 2D boron sheets is that some of these sheets have been experimentally synthesized on Ag substrates [23,24]. It is expected that the electronic and mechanical properties of the boron sheets can be modulated, as demonstrated in MgB_2 [25], BeB_2 [26], and TiB_2 [27].

*cheng.lu@unlv.edu
†liangzhi.kou@qut.edu.au
‡chen@physics.unlv.edu

In this work, we explore cobalt decorated boron sheets using an advanced structure search method combined with first-principles energetic and dynamic calculations. Our results identify a stable 2D CoB_6 monolayer that exhibits strong intrinsic ferromagnetism with high stability and an intriguing electronic structure that hosts Dirac cone structures with linear dispersions. The identified planar structure and the associated magnetic order remain robust against the adsorption of common molecules present in the ambient environment, and an externally applied tensile strain is able to effectively tune and enhance the ferromagnetic stability and moment. We propose two feasible approaches for synthesizing the predicted CoB_6 monolayer, namely by Co adsorption on the reportedly proposed δ_4 boron framework, or by direct chemical growth, which is supported by our extensive calculations on the stability of planar $Co_4B_8^+$ molecular clusters. The high structural and ferromagnetic stabilities of the CoB_6 monolayer, together with the strain tunable and enhanced magnetism and highly feasible experimental synthesis, are expected to stimulate efforts to further study and develop this fascinating 2D ferromagnetic material. The present findings lay a strong physics foundation for additional pertinent researches.

II. COMPUTATIONAL METHODS

Our structure prediction for Co_xB_y ($x, y = 1$–6) monolayer is based on a global minimum search of the free energy surfaces by the CALYPSO method [28–30]. The significant feature of this method is its capability of predicting both the ground-state and metastable structures with only the knowledge of the given chemical composition. Its validity has been confirmed by successful predictions of a diverse variety of materials [31–41]. The evolutionary variable cell structure prediction is performed, with each generation containing 30 structures, among which 60% are generated by particle-swarm optimization (PSO) while the others are new and generated randomly. We followed 50 generations to achieve the converged structure. The candidate structures of each composition are fully relaxed until their energy and force are converged to 10^{-6} eV and 0.001 eV/Å, respectively, by using the Vienna *Ab initio* Simulation Package (VASP) code [42]. The projector-augmented wave (PAW) [43] approach is adopted to represent the ion-electron interaction. The generalized gradient approximation (GGA) in the form of the Perdew-Burke-Ernzerhof (PBE) [44] functional has been employed with an energy cutoff of 500 eV for the plane-wave expansion. To check the influence of the correlation effect introduced by the Co $3d$ electrons, we performed PBE+U calculations ($U = 3.5$ or 6.0 eV), and also used the screened hybrid Heyd-Scuseria-Ernzerhof (HSE06) [45,46] functional to determine the electronic band structure. A vacuum space of at least 15 Å has been introduced to avoid the interaction between periodic images. A Monkhorst-Pack k-point mesh of $13\times5\times1$ is used for the sampling of the Brillouin zone during the geometry optimization. A phonon dispersion analysis is performed using the PHONOPY code [47] to examine the dynamical stability of the CoB_6 monolayer. Thermal stability of the predicted CoB_6 2D structure has been checked using *ab initio* molecular dynamics (AIMD) simulations, and the Nosé-Hoover method [48] was used based on the PAW method and PBE functional. The diffusion energy of the Co atoms on the δ_4 boron sheet is calculated by the climbing-image nudged elastic band (CI-NEB) method [49].

III. RESULTS AND DISCUSSION

A. Geometric structure of the CoB_6 monolayer

We examined over 1000 Co_xB_y ($x, y = 1$–6) structures based on the PSO structure search; all these structures were fully relaxed using the VASP code [42], and their dynamical stabilities were then checked by phonon calculations. This extensive and systematic process identifies the global ground-state CoB_6 monolayer shown in Fig. 1(a). In this fully optimized structure, the CoB_6 sheet is completely planar with a single atomic layer thickness, and the relaxed lattice constants are $a = 2.904$ Å, $b = 7.694$ Å. Each Co atom coordinates with six surrounding B atoms and the optimized Co-B bond lengths range from 2.022 to 2.118 Å. From these structural characteristics, the CoB_6 monolayer can be viewed as having Co atoms uniformly embedded in the δ_4 boron sheet [50]. This structure, however, is distinct from the recently

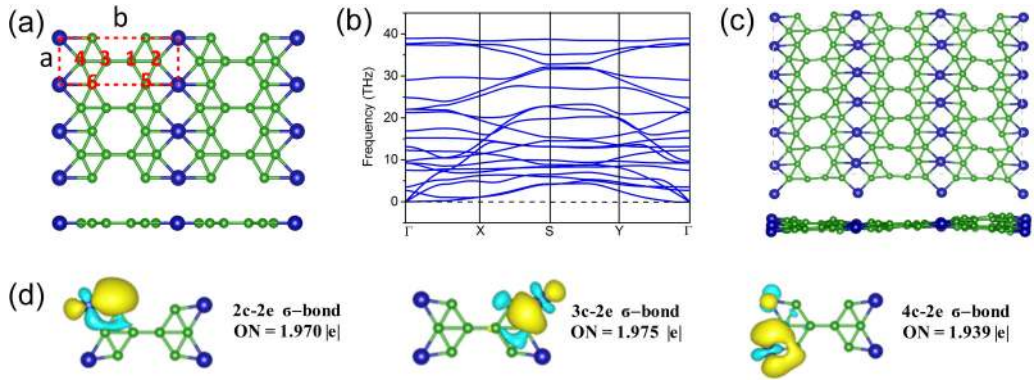

FIG. 1. (a) Top and side views of the CoB_6 monolayer. The blue and green spheres represent Co and B atoms, respectively. (b) Calculated phonon dispersion of the CoB_6 monolayer. (c) Snapshots of the CoB_6 monolayer at 500 K at the end of 1.5 ps of AIMD simulations. (d) The chemical bonding picture of the $Co_4B_8^+$ molecule obtained using the AdNDP method. Here ON denotes the occupation number.

proposed FeB_6 layered structure where Fe atoms occupy the hexagonal centers of the graphene-like boron sheet [51] or the MnB_6 layered structure where Mn atoms are sandwiched between two boron layers [20].

B. Thermodynamic, kinetic, and thermal stability of the COB_6 monolayer

To further evaluate the energetics of the CoB_6 monolayer, we first assess its cohesive energy $E_{coh} = (E_{Co} + 6E_B - E_{CoB_6})/7$, where E_{Co}, E_B, and E_{CoB_6} are the total energies of an isolated Co atom, an isolated B atom, and one unit cell of the CoB_6 monolayer, respectively. The calculated E_{coh} of the monolayer CoB_6 is 5.84 eV/atom, which is higher than those of Be_2C (4.86 eV/atom) [52] and FeB_6 (5.56-5.79 eV/atom) [51] at the same computational level. Although the stability of these materials cannot be directly compared by their cohesive energies due to differences in the nature of bonding configurations in different materials, this result still serves as a good indication that the CoB_6 monolayer is a strongly bonded 2D network. Dynamical stability of the CoB_6 monolayer is confirmed by calculating its phonon dispersion. Results in Fig. 1(b) show no imaginary frequency in the entire first Brillouin zone. It is noted that the highest frequency of this CoB_6 monolayer reaches up to 39.05 THz ($\approx$1303 cm^{-1}), which is much higher than the highest frequencies of Cu_2Si (420 cm^{-1}) [53], MoS_2 sheet (473 cm^{-1}) [54], or TiC monolayer (810 cm^{-1}) [55], indicating the strong Co-B and B-B chemical bonding in this predicted CoB_6 sheet. We further verified the thermal stability of the CoB_6 monolayer by performing AIMD simulations at 500 K using a 5×3 supercell. Snapshots taken at the end of a 1.5 ps simulation period [see Fig. 1(c)] with a time step of 1 fs show that the framework of the planar sheet is generally well preserved. These systematic tests show that the predicted CoB_6 monolayer is energetically, dynamically, and thermally stable.

C. Stabilization mechanism

To better understand the nature of the bonding in the CoB_6 monolayer, we first check the electron redistribution. A Bader charge analysis confirms that each Co atom donates 0.38e to B atoms (see Table S1 of the Supplemental Material [56] for more details), which indicates that Co atoms are ionized, thus helping to stabilize the boron-sheet framework. We also examine its molecular building block to understand the structural stability of the predicted CoB_6 monolayer. We used the CALYPSO code to search and screen a large number of Co_xB_y clusters, and we identified a minimum-energy $Co_4B_8^+$ cluster (Fig. S1 [56]), which possesses a planar structure with D_{2h} symmetry and can serve as a precursor for the 2D CoB_6 monolayer. From the natural electron configurations and a Wiberg bond index analysis, we find strong covalent interactions between the Co and B atoms and covalent characteristics of the B_8 framework (Figs. S2 and S3, Table S2 [56]) in this cluster. An adaptive natural density partitioning (AdNDP) analysis reveals the coexistence of 2c-2e (2 center–2 electron), 3c-2e, and 4c-2e σ-bond (Fig. 1(d) and Figs. S2 [56]) bonding configurations, which help to stabilize the planar $Co_4B_8^+$ cluster as well as the CoB_6 monolayer, similar to the situation in α-boron sheets [57].

D. Magnetic and electronic properties

It is expected that the partially filled Co 3d shell should lead to a magnetically ordered state in the CoB_6 monolayer structure. To explore this scenario, we first calculated the magnetic anisotropy energy (MAE) to determine the easy axis of possible ferromagnetic states. Within the PBE functional with the inclusion of the spin-orbit coupling (SOC), it is found that the easy axis initially placed in the basal plane [(i.e., the (100) or (010) plane] would automatically switch to align in the c, or (001), direction during self-consistent calculations, indicating that the easy axis has a strong preferential orientation along the out-of-plane direction. We then determined the preferred coupling of magnetic orders by comparing the total energies using a 2×1 supercell for three different magnetic configurations: ferromagnetic (FM) state, antiferromagnetic (AFM) state, and nonmagnetic (NM) state. Calculated results show that the FM configuration lies 77 and 114 meV lower in energy than the AFM and NM configurations, respectively, indicating that monolayer CoB_6 has a FM ground state. The occurrence of FM ground states can be also understood in terms of the Stoner criterion, which is described as $N(E_F)I > 1$, where $N(E_F)$ denotes the DOS at the Fermi level of the NM structure and I is the exchange integral. According to our calculated DOS and band structure in NM states (see Fig. S4 [56]), localized and high peaks of DOS near the Fermi level, which are mainly contributed by Co 3d electrons, can be observed. The broad density of the sharp peak around the Fermi level indicates the extreme instability of NM states, leading to the spin splitting. Thus the magnetic moments on the Co sites are formed. Meanwhile the calculations for possible Fermi surface nesting indicate FM is stable (Fig. S5) [56]. Spin-polarized electronic calculations indicate that the magnitude of the magnetic moment is 0.94μ_B per formula unit, and the spin unpaired electrons are mainly localized on the Co atoms [see Fig. 2(a)]. The on-site Coulomb interactions among the Co 3d electrons play a significant role in determining the electronic properties. Our PBE+U calculations show that the FM state is further stabilized and lower in energy by 328 and 344 meV than the AFM state (for more details see Table S3 [56]), with enhanced magnetic moments of 1.377μ_B and 1.382μ_B per Co atom, respectively, at the U values of 3.5 and 6.0 eV. It is seen that while the correlation effects influence the magnetic moment and stability, their main influence is to enhance the FM ground state.

We also calculated the spin-resolved density of states (DOS) and the corresponding electronic band structures. The states at the Fermi level [Fig. 2(c)] are predominantly contributed by the Co d electrons, and this result is consistent with the spin-polarized electron distribution shown in Fig. 2(a). The spin-polarized band structures [see Figs. 2(b) and 2(d)] also reveal considerable asymmetric spin states near the Fermi level. The spin-down channel is metallic while the spin-up channel possesses two Dirac cones [Fig. 2(d)] with linear dispersions in the vicinity. Both of these Dirac cones are located near the Fermi level with slight gap openings. The energy bands near the two Dirac points exhibit linear dispersions

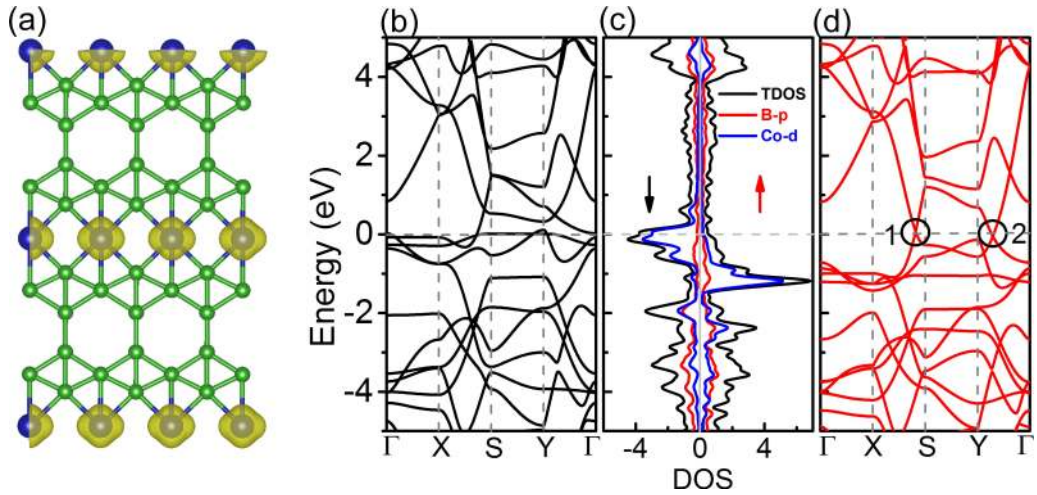

FIG. 2. (a) The spin-unpaired charge distribution on the CoB_6 monolayer (isosurface level: 0.005 $e/Å^3$). (b) Spin-polarized band structure for the spin-down channel. (c) Total and projected DOS. (d) Spin-polarized band structure for the spin-up channel. The Fermi level is set to zero in (b) and (d).

along the X-S and Y-Γ directions, and the associated Fermi velocities are in the range of $(4.25–9.20)\times10^5$ m/s, which are on the same order compared with graphene [58]. These Dirac cones persist in the electronic band structures produced by the HSE calculations (Fig. S6 [56]) and PBE+U calculations although they are shifted downwards to the valance band area, and an additional quadratic band is at the same level (Fig. S7 [56]).

E. Effects of strain and environment

The intriguing electronic and magnetic properties of the CoB_6 monolayer originate from the B-B and B-Co bonding configurations, which can be tuned by applied strain [59–62]. Here we focus on the influence of tensile strains, since compressive strains tend to buckle 2D materials [63,64]. Figure 3(a) shows the magnetic moment and Co-Co distance as a function of an external biaxial tensile strain, which causes a significant increase of the magnetic moment, monotonically rising from $1.9\mu_B$ to $2.8\mu_B$ per supercell at up to 10% strain under the PBE calculations. Meanwhile, the ferromagnetic stabilities of the CoB_6 monolayer are also remarkably enhanced, as evidenced by the increased energy differences with other states. As illustrated in Fig. 3(b), $\Delta E_1(E_{\rm AFM}-E_{\rm FM})$ exhibits a significant increase from 77 to 151 meV and $\Delta E_2(E_{\rm NM}-E_{\rm FM})$ dramatically increases up to 575 meV at 10% strain, which represents an approximately 400% enhancement. Under an uniaxial tensile strain, similar results were obtained at strains up to 4% (see Fig. S8 [56]). The applied strains also affect the spin-polarized electronic band structures, but the Dirac cone structures remain (Figs. S9 and S10 [56]).

The strain enhanced ferromagnetic stability can be understood within the Goodenough-Kanamori-Anderson (GKA) rules [65–67]. From the bonding structures illustrated in the inset of Fig. 3(a), it is seen that the ferromagnetic coupling strength is governed by two exchange interactions: a short-range direct nearest-neighbor d-d exchange ($J_{\rm D}$) and a superexchange via boron p states ($J_{\rm S}$) [68]. The direct d-d exchange originates from the Co d orbitals, and it is in AFM coupling with $J_{\rm D}<0$ and is sensitive to the variation of the distance between the adjacent Co atoms. In contrast, since the angle of Co-B-Co (92°) is close to 90°, the d orbitals on the nearest-neighbor Co atoms overlap with the p orbitals of B atoms and are orthogonal to each other. Consequently, the superexchange mediated by the boron atom is in FM order with $J_{\rm S}>0$ according to the GKA rules. The superexchange strength is thus mainly sensitive to the Co-B-Co angle. The different responses of the two exchange parameters lead to a modulation of the magnetic stability under tensile strains, as the overall coupling is determined by $J_{\rm D}+J_{\rm S}$. Under biaxial tensile strains, the Co-B-Co angle stays almost unchanged (around 90°) although the Co-B bonding distance is increased. As a result, the FM superexchange interaction ($J_{\rm S}$) is less affected by strains. However, the AFM coupling originating from the direct d-d exchange is significantly weakened, with the value of $|J_{\rm D}|$ deceasing dramatically as the Co-Co distance is appreciably increased, at a rate much faster than that for the Co-B distance. Consequently, the resulting coupling becomes decisively more ferromagnetic under increasing tensile strains.

In practical applications, monolayer CoB_6 will likely be in contact with the ambient environment, which may alter the electronic and magnetic properties. Here, we consider the adsorption of common air components O_2, CO_2, and H_2O on the CoB_6 monolayer to examine the robustness of its main properties. Several possible adsorption positions of gas molecules on the 2×2 CoB_6 monolayer have been examined, and the most favorable adsorption geometries are shown in Figs. 4(a)–4(c). We find that the O_2 molecule is bridged between two Co atoms with an adsorption distance of 1.96 Å, and the CoB_6 sheet becomes slightly buckled, indicating the nature of chemisorption [see Fig. 4(a)]. The corresponding DOS in Fig. 4(d) clearly shows that the $2p$ orbitals of O atoms make strong contributions to the states near the Fermi level. This chemical bonding interaction between O_2 and the CoB_6 monolayer remarkably modifies the electronic properties (Fig. S9); however, ferromagnetism is well preserved

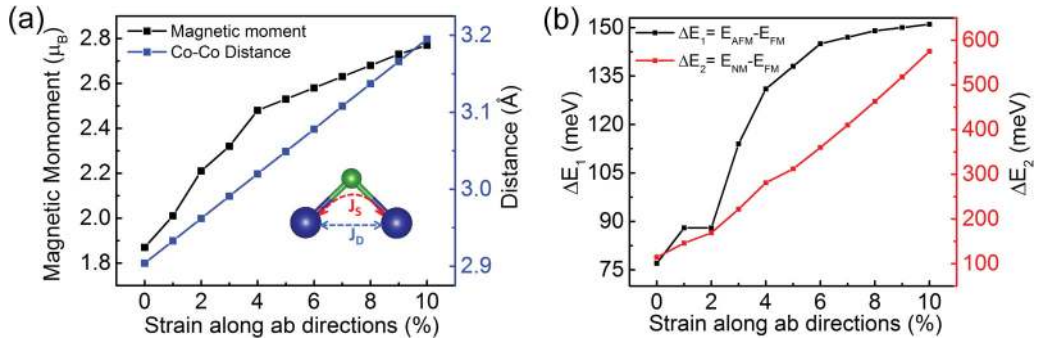

FIG. 3. (a) Magnetic moment per (2×1) supercell (black line) and nearest Co-Co distance (blue line). (b) Energy differences ΔE_1 (black line) and ΔE_2 (red line) per (2×1) supercell as a function of biaxial tensile strains along the *a* and *b* directions.

and the magnetic moment is actually increased due to the contribution from oxygen (from $0.94\mu_B$ to $1.31\mu_B$ per CoB_6 unit), indicating that the oxygen environment is favorable for strong ferromagnetism in the CoB_6 monolayer. In contrast, CO_2 and H_2O are obviously physisorbed on monolayer CoB_6 with distances of 3.36 and 2.24 Å, respectively, and the structure of the host is little affected [Figs. 4(b) and 4(c)]. The corresponding DOS from the adsorbed molecules stay far away from the Fermi level [Figs. 4(e) and 4(f)], and the magnetic moment remains nearly the same as in the pristine CoB_6 monolayer (Fig. S11 [56]). These results show that the ferromagnetic ground state of the CoB_6 monolayer can survive, and even thrive, in the ambient environment.

F. Feasible synthesis routes

We finally examine and propose two feasible synthesis routes for the predicted CoB_6 monolayer. The first is based on the recently proposed boron nanosheet [23,24,69]. From its configurational characteristics, the CoB_6 monolayer can be viewed as a combination of Co atoms and the δ_4 boron framework [Fig. 5(a)], with the sheet having a vacancy density of $\eta = 1/4$ as discussed in a previous report [49]. It is noted that even though the cohesive energy of the δ_4 boron sheet is a little higher than an experimentally synthesized β_{12} and χ_3 monolayer [24], it is lower than that of a recently fabricated graphene-like boron sheet [69], thus showing great potential to be obtained in experiment. We propose to synthesize monolayer CoB_6 via depositing Co atoms on the δ_4 boron sheet. To determine the preferred adsorption position, Co atoms are initially placed on seven possible sites of the boron network [see Fig. 5(a)]. Adsorption energy calculations ($E_{ads} = E_{Co} + E_{\delta_4} - E_{Co\text{-}\delta_4}$) show that the most preferred adsorption site for the Co atoms is the hexagon center of the δ_4 boron sheet [see inset in Fig. 5(b)]. The embedding of Co atoms significantly expands the lattice constant along the *b* direction and immerses Co atoms into the boron sheet plane, leading to the atomic thick monolayer CoB_6 structure. During the structural relaxation, the total energy linearly decreases without any energy barrier and the lattice along the *b* direction is automatically expanded by 16% as shown in Fig. 5(d). When Co atoms are initially adsorbed on other positions [1, 2, 3, 5, and 7; see Fig. 5(a)], they are in metastable states, and the associated adsorption energies are much lower. The results of our CI-NEB calculations show that the Co atoms will diffuse to the hollow position after overcoming a reasonably low energy barrier of 0.33 eV [Fig. 5(c)], and the structure will then automatically expand into the CoB_6 monolayer [Fig. 5(d)]. These results indicate that the atomic thin CoB_6 monolayer can be fabricated by depositing Co

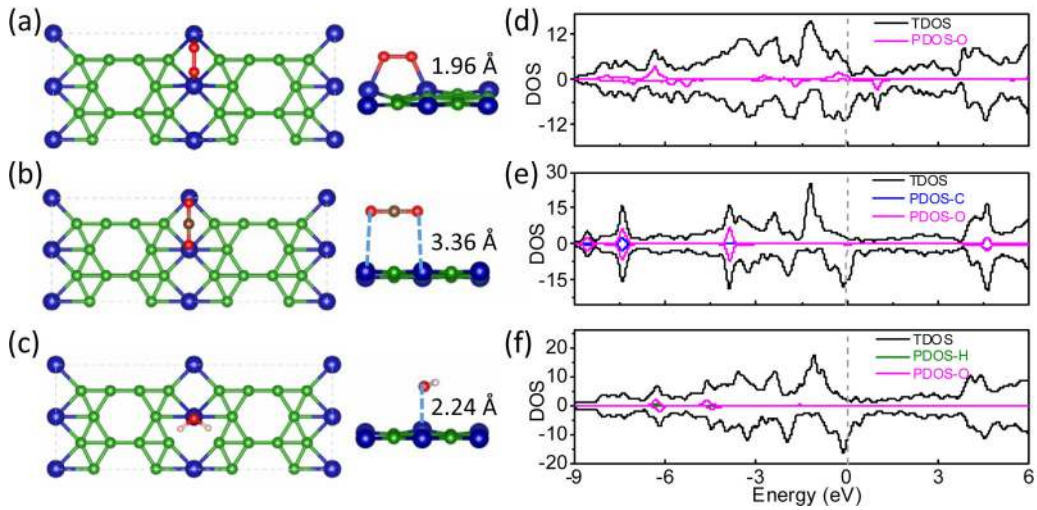

FIG. 4. (a)–(c) Top and side views and (d)–(f) calculated electronic DOS of O_2, CO_2, and H_2O adsorbed CoB_6 monolayers.

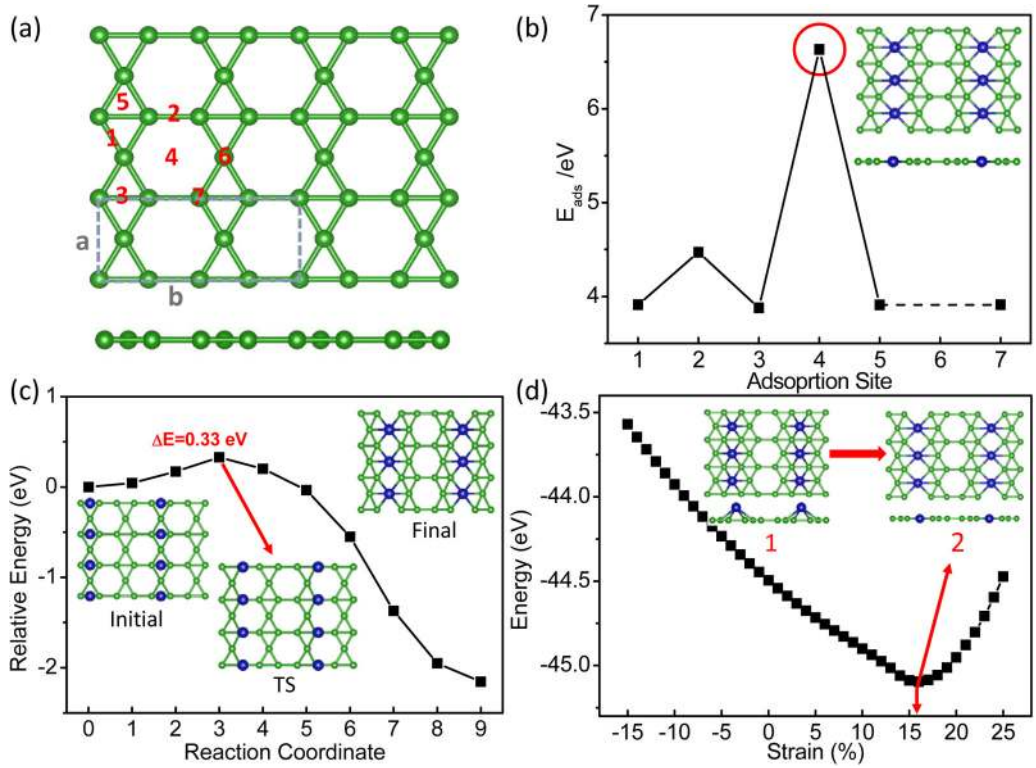

FIG. 5. (a) The geometry of the δ_4 boron sheet and seven initial positions for Co adsorption. (b) Adsorption energies and the lowest energy configuration of the Co-adsorbed δ_4 boron sheet; a Co atom initially placed at position 6 will automatically relax to position 4, thus positions 5 and 7 are connected by a dashed line. (c) Kinetic energy barrier from position 3 to position 4 from CI-NEB calculations; insets show initial, transition state, and final configurations. (d) The total energy of optimized structures as a function of strain; insets show the initial geometry and the lowest energy configuration.

atoms on the δ_4 boron sheet. Alternatively, it is also possible to a fabricate CoB_6 monolayer via direct chemical growth, based on our cluster calculations. Since the planar $Co_4B_8^+$ cluster is structurally stable, it is expected to be a highly efficient precursor for growing the CoB_6 monolayer. However, precise synthesis details such as the optimal pressure and temperature conditions will have to be further explored experimentally.

IV. CONCLUSION

Our extensive structure search in conjunction with first-principles energetic, dynamic, and thermodynamic calculations has uncovered a 2D CoB_6 monolayer that exhibits strong intrinsic ferromagnetism. This atomic thin planar ferromagnet hosts a robust ferromagnetic ground state with a large magnetic moment that can be effectively tuned and considerably enhanced by applied tensile strains. The ferromagnetic state remains stable upon the adsorption of common air components O_2, CO_2, and H_2O. Electronic band structure calculations reveal remarkable Dirac cone features with characteristic linear dispersions and high Fermi velocities. Our study introduces an outstanding candidate material into the family of intrinsic 2D ferromagnets, and provides a strong physics foundation for elucidating the structural, electronic, and magnetic properties as well as possible synthesis routes. The present results offer crucial guidelines for realizing and implementing the CoB_6 monolayer as a promising component for magnetoelectric devices.

ACKNOWLEDGMENTS

We acknowledge the grants of high-performance computer time from the computing facility at the Queensland University of Technology, the Pawsey Supercomputing Centre, and Australian National Facility. L.K. gratefully acknowledges financial support by the ARC Discovery Early Career Researcher Award (DE150101854).

[1] I. Žutić, J. Fabian, and S. Das Sarma, Rev. Mod. Phys. **76**, 323 (2004).
[2] Y. J. Sun, Z. W. Zhuo, X. J. Wu, and J. L. Yang, Nano Lett. **17**, 2771 (2017).
[3] H. Kumar, N. C. Frey, L. Dong, B. Anasori, Y. Gogotsi, and V. B. Shenoy, ACS Nano **11**, 7648 (2017).
[4] Y. G. Zhou, Z. G. Wang, P. Yang, X. T. Zu, L. Yang, X. Sun, and F. Gao, ACS Nano **6**, 9727 (2012).
[5] H. González-Herrero, J. M. Gómez-Rodriguez, P. Mallet, M. Moaied, J. J. Palacios, C. Salgado, M. M. Ugeda, J. Y. Veuillen, F. Yndurain, and I. Brihuega, Science **352**, 437 (2016).

[6] B. Uchoa, V. N. Kotov, N. M. R. Peres, and A. H. Castro Neto, Phys. Rev. Lett. **101**, 026805 (2008).

[7] J. Zhou, Q. Wang, Q. Sun, X. S. Chen, Y. Kawazoe, and P. Jena, Nano Lett. **9**, 3867 (2009).

[8] C. Gong, L. Li, Z. L. Li, H. W. Ji, A. Stern, Y. Xia, T. Cao, W. Bao, C. Z. Wang, Y. Wang, Z. Q. Qiu, R. J. Cava, S. G. Louie, J. Xia, and X. Zhang, Nature (London) **546**, 265 (2017).

[9] K. L. Seyler, D. Zhong, D. R. Klein, S. Y. Gao, X. O. Zhang, B. Huang, E. Navarro-Moratalla, L. Yang, D. H. Cobden, M. A. McGuire, W. Yao, D. Xiao, P. Jarillo-Herrero, and X. D. Xu, Nat. Phys. **14**, 277 (2018).

[10] B. Huang, G. Clark, E. Navarro-Moratalla, D. R. Klein, R. Cheng, K. L. Seyler, D. Zhong, E. Schmidgall, M. A. McGuire, D. H. Cobden, W. Yao, D. Xiao, P. Jarillo-Herrero, and X. D. Xu, Nature (London) **546**, 270 (2017).

[11] M. Bonilla, S. Kolekar, Y. J. Ma, H. C. Diaz, V. Kalappattil, R. Das, T. Eggers, H. R. Gutierrez, M. H. Phan, and M. Batzill, Nat. Nanotechnol. **13**, 289 (2018).

[12] S. W. Jiang, L. Z. Li, Z. F. Wang, K. F. Mak, and J. Shan, Nat. Nanotechnol. **13**, 549 (2018).

[13] B. Huang, G. Clark, D. R. Klein, D. MacNeill, E. Navarro-Moratalla, K. L. Seyler, N. Wilson, M. A. McGuire, D. H. Cobden, and D. Xiao, Nat. Nanotechnol. **13**, 544 (2018).

[14] L. F. Li, C. Xu, B. K. Jin, and L. J. Cheng, J. Chem. Phys. **139**, 1743102 (2013).

[15] C. Romanescu, T. R. Galeev, W. L. Li, A. I. Boldyrev, and L. S. Wang, Angew. Chem. Int. Ed. **50**, 9334 (2011).

[16] W. L. Li, C. Romanescu, T. R. Galeev, Z. A. Piazza, A. I. Boldyrev, and L. S. Wang, J. Am. Chem. Soc. **134**, 165 (2012).

[17] C. Romanescu, T. R. Galeev, W. L. Li, A. I. Boldyrev, and L. S. Wang, Accounts. Chem. Res. **46**, 350 (2013).

[18] S. G. Xu, Y. J. Zhao, X. B. Yang, and H. Xu, Rsc. Adv. **7**, 30320 (2017).

[19] X. Zhang, Z. H. Zhang, X. D. Zhao, D. H. Wu, and Z. Zhou, FlatChem **4**, 42 (2017).

[20] J. Li, X. Y. Fan, Y. P. Wei, J. X. Liu, J. H. Guo, X. X. Li, V. Wang, Y. Y. Liang, and G. Chen, J. Mater. Chem. C **4**, 10866 (2016).

[21] I. A. Popov, T. Jian, G. V. Lopez, A. I. Boldyrev, and L. S. Wang, Nat. Commun. **6**, 86544 (2015).

[22] W. L. Li, X. Chen, T. Jian, T. T. Chen, J. Li, and L. S. Wang, Nat. Rev. Chem. **1**, 0071 (2017).

[23] A. J. Mannix, X. F. Zhou, B. Kiraly, J. D. Wood, D. Alducin, B. D. Myers, X. L. Liu, B. L. Fisher, U. Santiago, J. R. Guest, M. J. Yacaman, A. Ponce, A. R. Oganov, M. C. Hersam, and N. P. Guisinger, Science **350**, 1513 (2015).

[24] B. J. Feng, J. Zhang, Q. Zhong, W. B. Li, S. Li, H. Li, P. Cheng, S. Meng, L. Chen, and K. H. Wu, Nat. Chem. **8**, 563 (2016).

[25] H. Tang and S. Ismail-Beigi, Phys. Rev. B **80**, 134113 (2009).

[26] P. H. Zhang and V. H. Crespi, Phys. Rev. Lett. **89**, 056403 (2002).

[27] L. Z. Zhang, Z. F. Wang, S. X. Du, H. J. Gao, and F. Liu, Phys. Rev. B **90**, 161402 (2014).

[28] Y. C. Wang, J. Lv, L. Zhu, and Y. M. Ma, Phys. Rev. B **82**, 094116 (2010).

[29] Y. C. Wang, J. Lv, L. Zhu, and Y. M. Ma, Comput. Phys. Commun. **183**, 2063 (2012).

[30] Y. C. Wang, M. S. Miao, J. Lv, L. Zhu, K. T. Yin, H. Y. Liu, and Y. M. Ma, J. Chem. Phys. **137**, 224108 (2012).

[31] J. Lv, Y. C. Wang, L. Zhu, and Y. M. Ma, Phys. Rev. Lett. **106**, 015503 (2011).

[32] L. Zhu, H. Y. Liu, C. J. Pickard, G. T. Zou, and Y. M. Ma, Nat. Chem. **6**, 644 (2014).

[33] L. Zhu, H. Wang, Y. C. Wang, J. Lv, Y. M. Ma, Q. L. Cui, Y. M. Ma, and G. T. Zou, Phys. Rev. Lett. **106**, 145501 (2011).

[34] D. Zhou, Q. Li, Y. M. Ma, Q. L. Cui, and C. F. Chen, J. Phys. Chem. C **117**, 5352 (2013).

[35] Q. Li, D. Zhou, W. T. Zheng, Y. M. Ma, and C. F. Chen, Phys. Rev. Lett. **110**, 136403 (2013).

[36] M. Zhang, H. Y. Liu, Q. Li, B. Gao, Y. C. Wang, H. D. Li, C. F. Chen, and Y. M. Ma, Phys. Rev. Lett. **114**, 015502 (2015).

[37] Q. Li, D. Zhou, W. T. Zheng, Y. M. Ma, and C. F. Chen, Phys. Rev. Lett. **115**, 185502 (2015).

[38] D. Zhou, Q. Li, W. T. Zheng, Y. M. Ma, and C. F. Chen, Phys. Chem. Chem. Phys. **19**, 4560 (2017).

[39] C. Lu, Q. Li, Y. M. Ma, and C. F. Chen, Phys. Rev. Lett. **119**, 115503 (2017).

[40] C. Lu and C. F. Chen, J. Phys. Chem. Lett. **9**, 2181 (2018).

[41] C. Lu, M. Amsler, and C. F. Chen, Phys Rev. B **98**, 054102 (2018).

[42] G. Kresse and J. Furthmüller, Phys. Rev. B **54**, 11169 (1996).

[43] G. Kresse and D. Joubert, Phys. Rev. B **59**, 1758 (1999).

[44] J. P. Perdew, K. Burke, and M. Ernzerhof, Phys. Rev. Lett. **77**, 3865 (1996).

[45] J. Heyd, G. E. Scuseria, and M. Ernzerhof, J. Chem. Phys. **118**, 8207 (2003).

[46] J. E. Peralta, J. Heyd, G. E. Scuseria, and R. L. Martin, Phys. Rev. B **74**, 073101 (2006).

[47] A. Togo, F. Oba, and I. Tanaka, Phys. Rev. B **78**, 134106 (2008).

[48] G. J. Martyna, M. L. Klein, and M. Tuckerman, J. Chem. Phys. **97**, 2635 (1992).

[49] G. Henkelman, B. P. Uberuaga, and H. Jónsson, J. Chem. Phys. **113**, 9901 (2000).

[50] X. J. Wu, J. Dai, Y. Zhao, Z. W. Zhuo, J. L. Yang, and X. C. Zeng, ACS Nano **6**, 7443 (2012).

[51] H. J. Zhang, Y. F. Li, J. H. Hou, K. X. Tu, and Z. F. Chen, J. Am. Chem. Soc. **138**, 5644 (2016).

[52] Y. F. Li, Y. L. Liao, and Z. F. Chen, Angew. Chem. Int. Ed. **53**, 7248 (2014).

[53] L. M. Yang, V. Bačić, I. A. Popov, A. I. Boldyrev, T. Heine, T. Frauenheim, and E. Ganz, J. Am. Chem. Soc. **137**, 2757 (2015).

[54] A. Molina-Sánchez and L. Wirtz, Phys. Rev. B **84**, 155413 (2011).

[55] Z. H. Zhang, X. F. Liu, B. I. Yakobson, and W. L. Guo, J. Am. Chem. Soc. **134**, 19326 (2012).

[56] See Supplemental Material at http://link.aps.org/supplemental/10.1103/PhysRevB.99.045445 for details on the structural and electronic properties of $Co_4B_8^+$ molecule, and band structures and magnetism modulation of 2D CoB_6 monolayer.

[57] H. Tang and S. Ismail-Beigi, Phys. Rev. Lett. **99**, 115501 (2007).

[58] P. E. Trevisanutto, C. Giorgetti, L. Reining, M. Ladisa, and V. Olevano, Phys. Rev. Lett. **101**, 226405 (2008).

[59] Y. W. Son, M. L. Cohen, and S. G. Louie, Nano Lett. **7**, 3518 (2007).

[60] Y. D. Ma, Y. Dai, M. Guo, C. W. Niu, L. Yu, and B. B. Huang, Nanoscale **3**, 2301 (2011).

[61] F. Li, Z. H. Zhu, X. D. Yao, G. Q. Lu, M. W. Zhao, Y. Y. Xia, and Y. Chen, Appl. Phys. Lett. **92**, 102515 (2008).
[62] J. Zhou, Q. Wang, Q. Sun, and P. Jena, Phys. Rev. B **81**, 085442 (2010).
[63] J. Feng, X. F. Qian, C. W. Huang, and J. Li, Nat. Photon. **6**, 866 (2012).
[64] G. Plechinger, A. Castellanos-Gomez, M. Buscema, H. S. J. van der Zant, G. A. Steele, A. Kuc, T. Heine, C. Schüller, and T. Korn, 2D Mater. **2**, 015006 (2015).
[65] J. B. Goodenough, Phys. Rev. **100**, 564 (1955).
[66] J. Kanamori, J. Appl. Phys. **31**, S14 (1960).
[67] P. W. Anderson, Phys. Rev. **115**, 2 (1959).
[68] V. V. Kulish and W. Huang, J. Mater. Chem. C **5**, 8734 (2017).
[69] W. B. Li, L. J. Kong, C. Y. Chen, J. Gou, S. X. Sheng, W. F. Zhang, H. Li, L. Chen, P. Cheng, and K. H. Wu, Sci. Bull. **63**, 282 (2018).